

Kinetics of antimicrobial peptide activity measured on individual bacterial cells using high-speed atomic force microscopy

Georg E. Fantner¹, Roberto J. Barbero², David S. Gray¹ and Angela M. Belcher^{1,2*}

Observations of real-time changes in living cells have contributed much to the field of cellular biology. The ability to image whole, living cells with nanometre resolution on a timescale that is relevant to dynamic cellular processes has so far been elusive^{1,2}. Here, we investigate the kinetics of individual bacterial cell death using a novel high-speed atomic force microscope optimized for imaging live cells in real time. The increased time resolution (13 s per image) allows the characterization of the initial stages of the action of the antimicrobial peptide CM15 on individual *Escherichia coli* cells with nanometre resolution. Our results indicate that the killing process is a combination of a time-variable incubation phase (which takes seconds to minutes to complete) and a more rapid execution phase.

High-resolution atomic force microscopy (AFM) images of live cells³ and cell fragments⁴ have resolved the nanoscale structure of cell walls⁵, the structural dynamics of the germination of single spores⁶, the structural changes of bacteria treated with bactericidal enzymes⁷ and the location of specific binding sites⁸. One of the limitations that makes AFM unsuitable for studying many dynamic processes in cell biology⁹ is the long image acquisition time of several minutes for one high-resolution AFM image. Progress in AFM instrumentation has enabled imaging of single molecules at up to video rates, but this has been limited to application to small areas (hundreds of nanometres) and flat samples^{10–12}. We used a high-speed atomic force microscope specifically designed to bridge the gap between the improved AFM technology and the biologically relevant but challenging experiments of interest in cellular biology. The key benefit of this instrument is the combination of very soft but rapid imaging and a scan size large enough to monitor multiple cells simultaneously.

Imaging live bacteria in an aqueous environment is one of the most challenging of applications for AFM¹³. The force interaction between the cantilever tip and the sample is critical. If the force is too high, the bacteria are damaged or disconnected from the surface; if it is too low, information about the sample is lost. Maintaining this balance at high imaging speeds is achieved using prototype AFM components and micro-fabricated small cantilevers¹⁴ (having a mass that is approximately a thousand times smaller than that of conventional cantilevers) with integrated tips. These cantilevers have resonance frequencies in liquid at ~ 100 kHz and spring constants between 300 and 1,000 pN nm⁻¹. The higher resonance frequency and the lower mass, quality factor and spring constant enable the imaging speed in tapping mode to be increased while keeping the imaging forces on the bacteria low¹⁵. Figure 1a shows a scanning electron microscopy (SEM) image of the small cantilevers used in this research. The inset shows a comparison of these with a conventional cantilever (NPS-B, Veeco

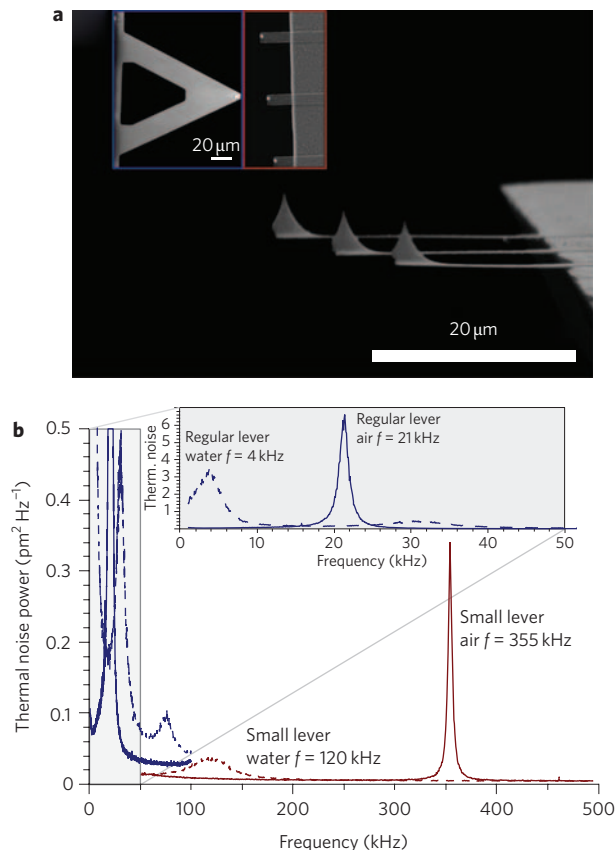


Figure 1 | Small AFM cantilevers for high-speed AFM. **a**, SEM image of small SiN cantilevers (~ 10 μm wide, 100–350 nm thick, 20–30 μm long). The inset compares the small levers (right) and a conventional lever (left) used for AFM imaging in fluid (Veeco NPS-D) at the same magnification. **b**, Thermal noise power spectra of regular and small cantilevers. In air (red solid line), the first resonance frequency of the small cantilever is ~ 355 kHz. In aqueous solution this drops to 100–120 kHz (red dashed line). The inset shows the thermal noise power spectra of an NP-S lever B with resonance frequencies of 21 kHz in air (blue solid line) and 4 kHz in aqueous solution (blue dashed line).

Metrology). Figure 1b shows the thermal spectra of the two types of cantilever. The resonance frequency of the small cantilever is 17 times higher than that of the conventional cantilever in air and is a factor of 30 greater in fluid.

¹Department of Materials Science and Engineering, Massachusetts Institute of Technology, Cambridge, Massachusetts 02139, USA, ²Department of Biological Engineering, Massachusetts Institute of Technology, Cambridge, Massachusetts 02139, USA. *e-mail: belcher@mit.edu

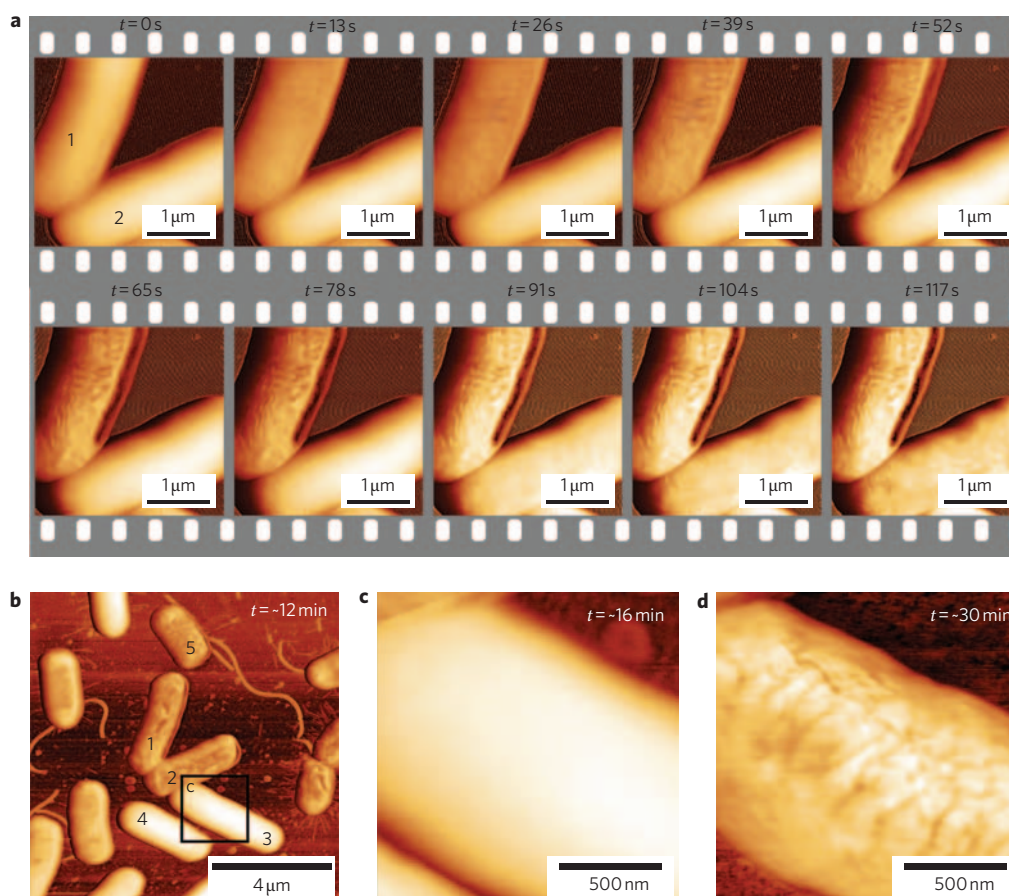


Figure 2 | *Escherichia coli* cell disruption induced by CM15, imaged with high-speed AFM. **a**, Time series of CM15 antimicrobial action. CM15 injected at $t = -6$ s and images recorded every 13 s, with a resolution of $1,024 \times 256$ pixels and a rate of 20 lines s^{-1} . The surface of the upper bacterium (1) starts changing within 13 s. The lower bacterium (2) resists changing for 78 s. **b**, Larger-area view recorded 12 min after addition of CM15. Most bacteria are corrugated, but some are still smooth. **c**, High-resolution image of bacterium 3 showing that this bacterium is still smooth at $t = 16$ min. **d**, Image of the now corrugated bacterium 3 at $t = 30$ min. Eventually, all bacteria in the field of view are affected by CM15. Images were recorded in liquid in tapping mode with a tapping frequency of 110 kHz. Phase images are shown here for high contrast; amplitude data are shown in Supplementary Fig. S2. Images **b-d** were recorded with a resolution of $1,024 \times 256$ pixels at 2 lines s^{-1} .

Antimicrobial peptides (AmPs) are a promising class of antimicrobials that have demonstrated activity against antibiotic-resistant bacteria, parasites, viruses and fungi^{16–19}. The high-speed AFM was used to measure the kinetics of the pre-death activity of a pore-forming, membrane-disrupting AmP (CM15) on individual live *Escherichia coli* cells in an aqueous solution²⁰.

Electron microscopy and AFM experiments have demonstrated the endpoint surface morphological changes of a population of cells treated with AmPs^{21–23}. Spectroscopic analyses of synthetic membranes or vesicles have provided insight into the sizes and structures of pores formed by AmPs^{24–26}. However, to date, the early-stage kinetics of the membrane-disrupting activity of an AmP on live cells have not been reported with a spatial resolution of nanometres and temporal resolution of seconds.

In this work, bacteria were immobilized on cover slides coated with poly-L-lysine. The bacteria were imaged in aqueous solution for at least 10 min to ensure that the cells were not altered or displaced by the AFM tip and to ensure that the poly-L-lysine did not change the cells in the timescales considered in our experiments. CM15 was added to the liquid droplet around the sample to a final concentration of $50 \mu\text{g ml}^{-1}$, or five times the minimum inhibitory concentration (MIC)²⁷. Images were acquired every 13 s.

Figure 2a shows AFM phase images of the surfaces of two bacteria before and at several time points after the addition of CM15. The most obvious effect of the addition of CM15 is a change in

the surface state of the bacteria from smooth to corrugated. AFM phase data are shown because the changes are most apparent there. The same changes in surface morphology are also visible in the AFM amplitude data (Supplementary Fig. S2). The changes are more difficult to discern in the AFM height data due to the large background variation on the surface of the bacteria. The changes in the surfaces of the bacteria are consistent with published electron microscopy data, which report ultra-structural damage to the outside of peptide-treated bacterial cells^{21–23}. Interestingly, there is a wide range in the time of onset of the change for individual bacteria. Bacterium 1 in Fig. 2a starts changing within 13 s of the addition of CM15, and the change is completed in ~ 60 s. Bacterium 2 does not start changing until ~ 80 s, and the change is not complete until ~ 120 s.

Figure 2b shows a larger area of the same sample 12 min after the addition of CM15 (bacteria 1 and 2 are in the centre of the image). Other bacteria (3 and 4) have still not changed. Figure 2c is a higher-resolution image of the smooth surface of bacterium 3, taken 16 min after the addition of CM15. Eventually, this bacterium (Fig. 2d) and indeed all bacteria in the field of view become corrugated. We considered several reasons for the cell-to-cell variation in onset time. The bacteria are all grown from a single clone, so we would expect them to be genetically identical. They are located close to one another (within $10 \mu\text{m}$), and are therefore exposed to the same concentration of CM15 at the same time. It is likely that the

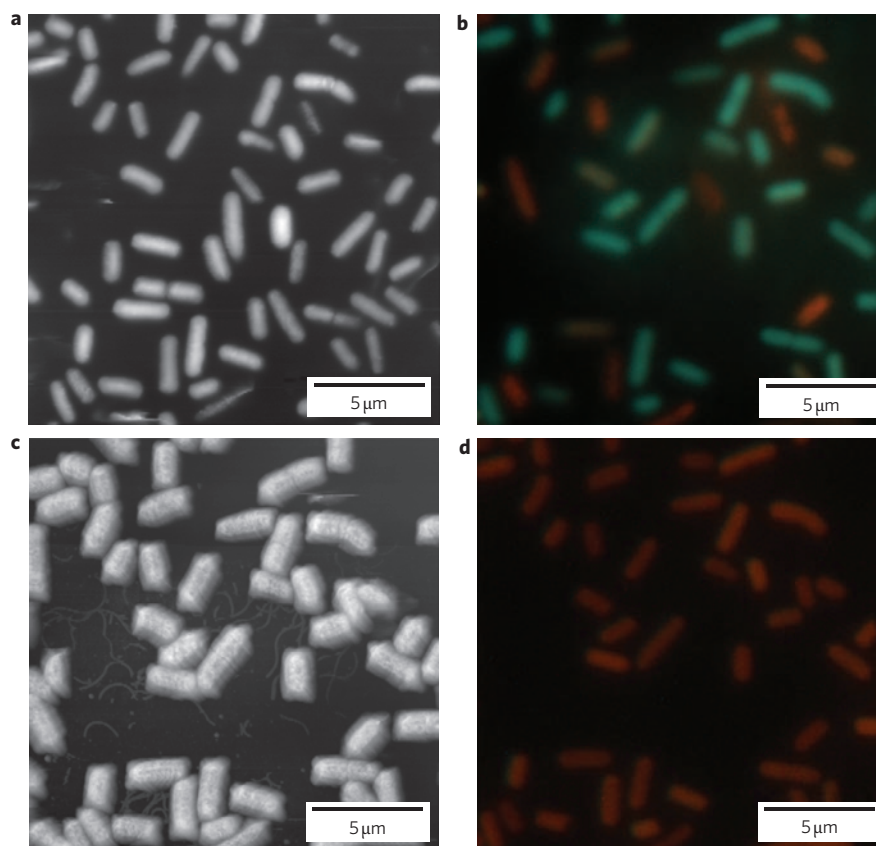


Figure 3 | AmP-induced surface morphology change correlates to cell death. Combined AFM and fluorescence microscopy images recorded on the same spot before and after addition of CM15. **a**, Tapping-mode image of bacteria before the addition of CM15 (phase data). The surfaces of most bacteria are smooth. **b**, Fluorescence image before the addition of CM15. Live bacteria, green; dead bacteria, red (LIVE/DEAD stain). **c**, AFM image 30 min after exposure to a CM15 solution at twice the MIC. Nearly all the bacteria have a corrugated surface. **d**, Fluorescence image after the addition of CM15. All bacteria are red, indicating that they are dead. AFM images were taken with a resolution of 512×256 pixels and a scan rate of 0.5 Hz.

cells are not all at the same stage in the cell cycle. However, in all of our experiments, we found no correlation between the time of onset of change and cell length (an indicator of the stage in the cell cycle²⁸).

To correlate the corrugation of the cell surface with cell death, we performed combined AFM and fluorescence microscopy using a fluorescent indicator of cell viability (LIVE/DEAD BacLight). Figure 3a presents an AFM image of live cells. To minimize disruptions caused by the AFM tip, the imaging force was reduced until only the tops of the bacteria were imaged. Figure 3b presents a fluorescence image of the same cells recorded immediately after AFM imaging. Figure 3c,d shows the AFM and fluorescence images of the same bacteria 30 min after the cells were exposed to a concentration of M15 equivalent to twice the MIC. Almost all of the bacteria have corrugated surfaces and there are no green (live) cells remaining. The apparent broadening of the cells is an imaging artefact due to the pyramidal shape of the tip²⁹. There was a strong correlation between the fluorescence and surface variation of the cells ($P < 0.004$). To ensure that the change was induced by the CM15, control experiments were performed with a positively charged peptide with no known antimicrobial action (Supplementary Fig. S4) and with the conventional antibiotic ampicillin (Supplementary Fig. S5).

The increased time resolution of the measurements allowed the characterization of the initial stages of antimicrobial action on individual live bacteria. The high-speed AFM experiment was repeated with a larger scan area to investigate relative differences in the response times of adjacent cells. At $t = 0$ s, the imaging solution was exchanged with a CM15 solution (twice the MIC) using

a flow-through system. One image was taken every 21 s; every fifth image is shown in Fig. 4a (for the full series see Supplementary Figs S6 and S7). It is evident that bacteria 1, 7 and 8 respond more quickly to the addition of CM15 than the other bacteria.

To quantify the kinetics of the change, we measured, for each bacterium separately, the change in the root-mean-square (r.m.s.) value of the surface corrugation along the long axis of the bacteria in every frame of the image. Figure 4b shows representative cross-sections through bacterium 1 for each image. The change in surface corrugation is visible ~ 80 s after the addition of CM15. Figure 4c shows the normalized r.m.s. corrugation values for the bacteria in Fig. 4a as a function of time after the addition of CM15. Time of onset of change is highly variable, in this experiment ranging from 40 s (bacterium 7) to more than 4 min (bacterium 2), with an average of 155 ± 89 s (mean \pm standard deviation). The time for each bacterium to complete the change (smooth to corrugated) is more consistent, with 50% of the damage completed within 52 ± 16 s. We chose phase data for the analysis, because the changes are most apparent. However, the same trends can be observed in the height and amplitude images (Supplementary Fig. S8). We monitored the CM15-treated cells for up to 100 min after treatment and did not observe any additional changes. Eventually, the cells disappear, but we cannot say whether this is due to lysis or due to the detachment of cells. Figure 4d shows the results of the measurement of the kinetics of CM15 activity on a population of cells. The bulk killing rate of CM15 can be described reasonably well with a single exponential with a half-time of 4.6 min.

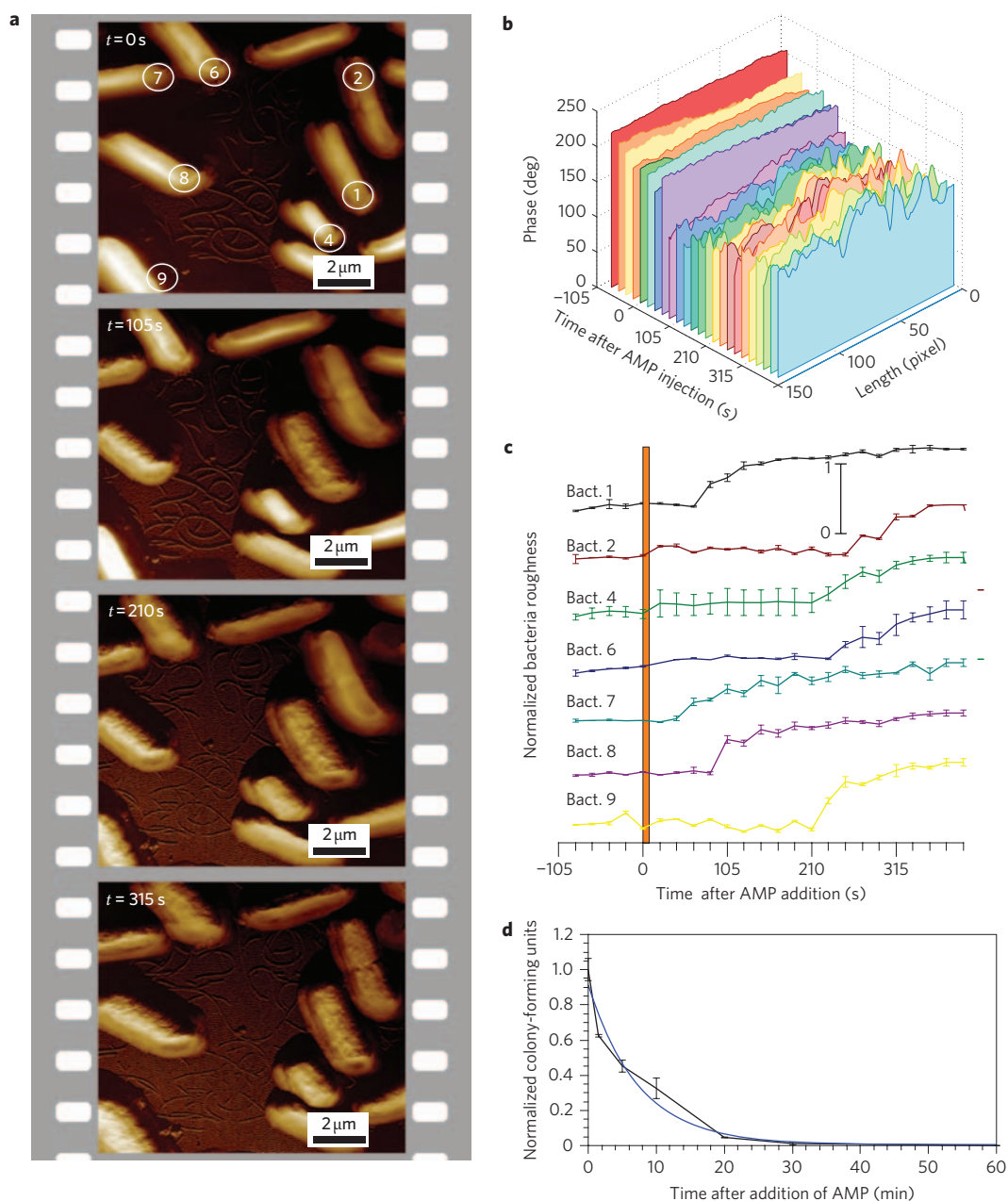


Figure 4 | Early-stage kinetics of CM15 action measured by AFM correlates with bulk killing activity experiment. **a** Time series of bacteria after injection of CM15. Images are recorded every 21 s ($1,024 \times 256$ pixels, 12.2 lines s^{-1}) with every fifth image shown (see Supplementary Information for the full time series). **b**, Cross-sections along the long axis of bacterium 1 showing the time progression of the surface variation. Each slice represents data extracted from one image in the full time series. **c**, Averaged surface variation of the bacteria as a function of time after injection of CM15 (bacteria numbers correspond to those in frame one of panel **a**). **d**, Bulk measurement of CM15 antimicrobial activity. The interpolated behaviour between 0 and 5 min correlates well with the single cell measurements.

With this AFM technique, one might expect to see the pores that are formed in the outer membrane by CM15. Unfortunately, the pores formed by CM15 are reported to have diameters of 2–4 nm (ref. 27), which is close to the pixel resolution of our high-speed images (4–10 nm, scan-size-dependent). Using a slower acquisition speed (2 lines s^{-1}), we obtained images for which the pixel resolution was 1 nm for a $1\text{-}\mu\text{m}$ image (Supplementary Fig. S3). Although there are features of this size in this higher-resolution image, we are reluctant to over-interpret the results.

We propose that the killing of the bacteria by CM15 is a two-stage process consisting of an incubation phase, which can last

from seconds to minutes, followed by an execution phase, in which 50% of the damage is completed in less than one minute. The time to complete the incubation phase varies considerably more from cell to cell than the time to complete the execution phase. This result suggests that the bulk kill rate is dominated by the time it takes to complete the incubation phase, rather than the execution phase. It also raises the question of whether the incubation and execution phases are prolonged equally in bacteria that are more resistant to AmPs or if one particular phase is more prolonged than the other. Answering this could be important for understanding the mechanism by which bacteria can develop resistance to this class of peptide antibiotics.

The heterogeneity in the dynamics of AmP-induced bacterial cell death has an interesting parallel in eukaryotic cell biology. Mammalian cell apoptotic death has recently been demonstrated to be a two-stage process comprising a time-variable and long-incubation phase followed by a more constant and relatively short execution phase³⁰. Despite the apparent differences in the overall mechanisms, protein/peptide-induced pore formation in a membrane is a critical component of both mammalian cell apoptotic death (mitochondrial outer membrane permeabilization) and AmP-induced bacterial cell death (outer membrane permeabilization).

Our observation of this two-stage process was made possible by the use of a high-speed AFM capable of recording dynamic changes on the single-cell level. These measurements demonstrate the enormous potential of high-speed AFM imaging for cellular biology. This technique can be applied to other cell types such as yeast or mammalian cells and even to eukaryotic cell organelles. The advances in AFM technology and its application reported here constitute an enabling technology with which cell biologists may explore cellular processes, in real time, at the nanometre level.

Materials and Methods

Antimicrobial peptide. We used a well-studied, pore-forming AmP called CM15 with the sequence KWKLFFKKGAVLKV. The peptide was made by Genscript using standard solid-phase peptide synthesis methods. It was purified by desalting and was shipped lyophilized. The peptide was resuspended and stored in Millipore water and diluted to the appropriate concentrations in Millipore water.

Bacteria preparation. *E. coli* bacteria (ATCC 25922) were grown overnight from a single colony in LB growth medium at 37 °C. Cells were diluted 1:100 in fresh LB medium and grown for 3 h. Cells were spun down and washed three times with Millipore water.

To increase adherence of the bacteria to the glass substrate, glass coverslips were coated with poly-L-lysine before depositing the bacteria. Round glass coverslips were boiled in 2.5 M HCl solution for 10 min to clean the glass. The coverslips were rinsed six times with Millipore water and then immersed for 10 min in a pH 8.0 solution of 0.05 mg ml⁻¹ poly-L-lysine hydrobromide (Sigma part number P1524) and 10 mM Tris. They were then covered and dried vertically overnight at room temperature. The coated coverslips were stored at room temperature and were used within one week.

Concentrated bacteria suspended in unbuffered Millipore water were deposited on the coated coverslips and incubated for 30 min. Excess cells were rinsed off with three washes of 1 ml Millipore water. Images were taken in Millipore water.

High-speed AFM imaging. All high-speed AFM images were taken on a customized AFM instrument based on a Veeco Multimode with a Nanoscope 5 controller (Veeco Metrology). The most enabling modifications were small cantilevers (SCL-Sensor.Tech. fabrication GesmbH) and a new AFM head designed for use with the small cantilevers (see Supplementary Fig. S1 for more details). We chose not to use a high-speed scanner for these experiments, because turnaround ripples and other distortions were small at these scanning parameters. All measurements were performed in tapping mode in fluid with an open fluid cell. Flow-through fluid exchange was achieved using a dual syringe pump. Height, amplitude and phase signals were recorded for both trace and retrace. The data were processed using ImageJ, ImageSXM and Gwyddion, using standard modification commands applied over the whole sample.

Combined AFM/fluorescence microscopy imaging. AFM images were recorded on a Digital Instruments Bioscope (Veeco Metrology) with an extended Nanoscope 3a controller, mounted on top of a Zeiss Axiovert 135 inverted microscope (Carl Zeiss Microimaging GmbH). AFM images were taken with a Veeco NPS cantilever in tapping mode (Veeco Instruments). Fluorescence images were recorded using a Zeiss ×100 Plan-Neofluar oil immersion objective and a Chroma Technology Corporation filter set 41012. Cells were stained with LIVE/DEAD BacLight stain (Invitrogen PN: L13152). The LIVE/DEAD stain was a mixture of SYTO[®] 9 green-fluorescent nucleic acid stain and propidium iodide red-fluorescent nucleic acid stain. These stains differ in their ability to penetrate healthy bacterial cells, with the green stain permeating healthy cells and the red stain permeating membrane-compromised cells.

Owing to the loss in viability during the preparation process, some cells were already dead before the commencement of the experiment (see Fig. 3b). During initial AFM imaging, some loosely connected cells detached from the surface, so not all cells in Fig. 3a are present in Fig. 3b.

Analysis of LIVE/DEAD stain results and correlation with r.m.s. variation of bacterial surfaces. Fluorescence images were analysed using ImageJ with nucleus

counter plug-in (downloaded from MacBiophotonics). Cells were identified and numbered using the nucleus counter plug-in. The colour images were split into red, green and blue channels. For each cell, the mean red and green values were measured and the green to red ratio for each cell calculated. The cells were divided into two populations, those with green to red ratios less than one (dead) and those with green to red ratios greater than one (live). Using the axial r.m.s. variation for each cell (calculation described below), a one-tailed Student's *t*-test was used to assess whether the live cell population and the dead cell population had statistically different r.m.s. variation values.

Calculation of axial r.m.s. variation of bacteria. To quantify the change in variations on the bacterial surface, line sections were extracted from the phase data on the top of each bacterium in the longitudinal direction. The exact number of line sections per bacterium per image depended on the size of the bacterium but was always more than 20. A third-degree polynomial was fit through each line section and subtracted from the original data. The resulting data represent only the higher spatial frequencies from which the r.m.s. value was calculated. The r.m.s. values of each line were then averaged over all the lines along the bacterium. This number represents one data point in Fig. 4c. The error bars represent standard deviations of this calculation when varying the exact area on each bacterium and the number of longitudinal sections used for the calculation. This calculation was repeated for each frame in the time series and for each cell. The data processing was carried out with custom software written in Labview and NI-Vision (National Instruments).

Bulk cell killing assay. Cells were grown overnight in LB from a single colony. In the morning, they were diluted 1:100 in fresh LB and grown for 3 h. After 3 h, they were washed three times in Millipore water. The washed cells were resuspended in Millipore water to a concentration of 2×10^6 cells ml⁻¹. The CM15 peptide was added to the cells to a final concentration of 20 μg ml⁻¹, which was the same peptide-to-cell ratio as that used in the AFM experiments. Aliquots were taken from the cells at various time points and were plated in triplicate on fresh, pre-warmed LB agar plates, which were incubated overnight at 37 °C. The number of colonies formed is an indicator of the number of viable cells remaining in the suspension at each time point. The number of colonies formed was counted and the average and standard deviation of each time point calculated. All data were normalized to the zero time point (before addition of peptide).

Received 11 November 2009; accepted 3 February 2010;
published online 14 March 2010

References

- Dufrene, Y. F. Using nanotechniques to explore microbial surfaces. *Nature Rev. Micro.* **2**, 451–460 (2004).
- Dufrene, Y. F. Towards nanomicrobiology using atomic force microscopy. *Nature Rev. Micro.* **6**, 674–680 (2008).
- Matzke, R., Jacobson, K. & Radmacher, M. Direct, high-resolution measurement of furrow stiffening during division of adherent cells. *Nature Cell Biol.* **3**, 607–610 (2001).
- Muller, D. J., Baumeister, W. & Engel, A. Controlled unzipping of a bacterial surface layer with atomic force microscopy. *Proc. Natl Acad. Sci. USA* **96**, 13170–13174 (1999).
- Muller, D. J., Fotiadis, D., Scheuring, S., Muller, S. A. & Engel, A. Electrostatically balanced subnanometer imaging of biological specimens by atomic force microscope. *Biophys. J.* **76**, 1101–1111 (1999).
- Plomp, M., Leighton, T. J., Wheeler, K. E., Hill, H. D. & Malkin, A. J. *In vitro* high-resolution structural dynamics of single germinating bacterial spores. *Proc. Natl Acad. Sci. USA* **104**, 9644–9649 (2007).
- Francius, G., Domenech, O., Mingeot-Leclercq, M. P. & Dufrene, Y. F. Direct observation of *Staphylococcus aureus* cell wall digestion by lysostaphin. *J. Bacteriol.* **190**, 7904–7909 (2008).
- Hintendorfer, P., Baumgartner, W., Gruber, H. J., Schilcher, K. & Schindler, H. Detection and localization of individual antibody–antigen recognition events by atomic force microscopy. *Proc. Natl Acad. Sci. USA* **93**, 3477–3481 (1996).
- Muller, D. J. & Dufrene, Y. F. Atomic force microscopy as a multifunctional molecular toolbox in nanobiotechnology. *Nature Nanotech.* **3**, 261–269 (2008).
- Ando, T. *et al.* A high-speed atomic force microscope for studying biological macromolecules. *Proc. Natl Acad. Sci. USA* **98**, 12468–12472 (2001).
- Kobayashi, M., Sumitomo, K. & Torimitsu, K. Real-time imaging of DNA–streptavidin complex formation in solution using a high-speed atomic force microscope. *Ultramicroscopy* **107**, 184–190 (2007).
- Hansma, P. K., Schitter, G., Fantner, G. E. & Prater, C. Applied physics—high-speed atomic force microscopy. *Science* **314**, 601–602 (2006).
- Dufrene, Y. F. Atomic force microscopy and chemical force microscopy of microbial cells. *Nature Protocols* **3**, 1132–1138 (2008).
- Fantner, G. E. *et al.* Components for high speed atomic force microscopy. *Ultramicroscopy* **106**, 881–887 (2006).
- Viani, M. B. *et al.* Fast imaging and fast force spectroscopy of single biopolymers with a new atomic force microscope designed for small cantilevers. *Rev. Sci. Instrum.* **70**, 4300–4303 (1999).

16. Tiozzo, E., Rocco, G., Tossi, A. & Romeo, D. Wide-spectrum antibiotic activity of synthetic, amphipathic peptides. *Biochem. Biophys. Res. Commun.* **249**, 202–206 (1998).
17. Gottlieb, C. T. *et al.* Antimicrobial peptides effectively kill a broad spectrum of *Listeria monocytogenes* and *Staphylococcus aureus* strains independently of origin, sub-type or virulence factor expression. *BMC Microbiol.* **8**, 205 (2008).
18. Hancock, R. E. W. & Sahl, H. G. Antimicrobial and host-defense peptides as new anti-infective therapeutic strategies. *Nature Biotechnol.* **24**, 1551–1557 (2006).
19. Loose, C., Jensen, K., Rigoutsos, I. & Stephanopoulos, G. A linguistic model for the rational design of antimicrobial peptides. *Nature* **443**, 867–869 (2006).
20. Andreu, D. *et al.* Shortened cecropin-a melittin hybrids—significant size-reduction retains potent antibiotic-activity. *FEBS Lett.* **296**, 190–194 (1992).
21. Kalfa, V. C. *et al.* Congeners of SMAP29 kill ovine pathogens and induce ultrastructural damage in bacterial cells. *Antimicrob. Agents Chemother.* **45**, 3256–3261 (2001).
22. Meincken, M., Holroyd, D. L. & Rautenbach, M. Atomic force microscopy study of the effect of antimicrobial peptides on the cell envelope of *Escherichia coli*. *Antimicrob. Agents Chemother.* **49**, 4085–4092 (2005).
23. Mangoni, M. L. *et al.* Effects of the antimicrobial peptide temporin L on cell morphology, membrane permeability and viability of *Escherichia coli*. *J. Peptide Sci.* **10**, 859–865 (2004).
24. Bechinger, B. The structure, dynamics and orientation of antimicrobial peptides in membranes by multidimensional solid-state NMR spectroscopy. *Biochim. Biophys. Acta Biomembranes* **1462**, 157–183 (1999).
25. Ladokhin, A. S., Selsted, M. E. & White, S. H. Sizing membrane pores in lipid vesicles by leakage of co-encapsulated markers: pore formation by melittin. *Biophys. J.* **72**, 1762–1766 (1997).
26. Lee, M. T., Hung, W. C., Chen, F. Y. & Huang, H. W. Mechanism and kinetics of pore formation in membranes by water-soluble amphipathic peptides. *Proc. Natl Acad. Sci. USA* **105**, 5087–5092 (2008).
27. Sato, H. & Feix, J. B. Osmoprotection of bacterial cells from toxicity caused by antimicrobial hybrid peptide CM15. *Biochemistry* **45**, 9997–10007 (2006).
28. Ferullo, D. J., Cooper, D. L., Moore, H. R. & Lovett, S. T. Cell cycle synchronization of *Escherichia coli* using the stringent response, with fluorescence labeling assays for DNA content and replication. *Methods* **48**, 8–13 (2009).
29. Alsteens, D. *et al.* Organization of the mycobacterial cell wall: a nanoscale view. *Pflug. Arch. Eur. J. Phys.* **456**, 117–125 (2008).
30. Albeck, J. G. *et al.* Quantitative analysis of pathways controlling extrinsic apoptosis in single cells. *Mol. Cell* **30**, 11–25 (2008).

Acknowledgements

The authors would like to thank T. Chau for helpful discussions about antimicrobial peptides. G.E.F. is supported by an Erwin-Schrödinger fellowship J2778-B12. R.J.B. is the recipient of a National Institutes of Health Biotechnology Training Program Fellowship. A.M.B. would like to thank the Massachusetts Institute of Technology for their generous support. This work was further funded by the Army Research Office through the Institute for Soldier Nanotechnology, the National Institute of Health under Award RO1 GM065354 and by the Austrian Research Promotion Agency under award no. VO156-08-BII: NSI-FABICAN.

Author contributions

G.E.F. and R.J.B. contributed to experimental design and execution and writing of the manuscript. D.S.G. designed the methods and sample preparation. A.M.B. contributed to experimental design, supervision and editing of the manuscript.

Additional information

The authors declare no competing financial interests. Supplementary information accompanies this paper at www.nature.com/naturenanotechnology. Reprints and permission information is available online at <http://npg.nature.com/reprintsandpermissions/>. Correspondence and requests for materials should be addressed to A.M.B.